

A Measurement of the Hubble Constant from the X-Ray Properties
and the Sunyaev-Zel'dovich Effect of CL 0016+16

John P. Hughes¹

Department of Physics and Astronomy, Rutgers University,
136 Frelinghuysen Road, Piscataway, NJ 08854-8019
E-mail: jph@physics.rutgers.edu

and

Mark Birkinshaw¹

Department of Physics, University of Bristol, Bristol, BS8 1TL, UK
E-mail: mark.birkinshaw@bristol.ac.uk

Received 17 February 1997; accepted __ January 1998

ABSTRACT

A value of the Hubble constant has been determined from a comparison of the X-ray properties and Sunyaev-Zel'dovich effect of the distant rich cluster of galaxies CL 0016+16. The cluster, as imaged by the *ROSAT* PSPC, is significantly elliptical and we present the techniques we have developed to include this in our analysis. Assuming a smooth, isothermal gas distribution, we obtain a value $H_0 = 47_{-15}^{+23} \text{ km s}^{-1} \text{ Mpc}^{-1}$, where the errors include systematic and random uncertainties but are purely observational. Systematic errors in deprojecting the elliptical surface brightness distribution due to prolate and oblate geometries as well as arbitrary inclination angles, introduce an additional fractional error of $\pm 17\%$ in H_0 . At the redshift of CL 0016+16 ($z = 0.5455$) the effect of the cosmological parameters on the derived H_0 value is of order 10%–20%; we quote results for $q_0 = 0.1$. Combining this result with X-ray/SZ-effect H_0 determinations from seven other clusters and taking account of systematic uncertainties in our models for the cluster atmosphere, we find an ensemble value of $H_0 = 42 - 61 \text{ km s}^{-1} \text{ Mpc}^{-1}$ with an additional random error of $\pm 16\%$.

Subject headings: cosmic microwave background – cosmology: observations – distance scale – galaxies: clusters: individual (CL 0016+16) – intergalactic medium

¹ Also Harvard-Smithsonian Center for Astrophysics, 60 Garden Street, Cambridge, MA 02138

1. INTRODUCTION

The Sunyaev-Zel'dovich (SZ) effect (Sunyaev & Zel'dovich 1972) offers the promise of directly measuring the distances to clusters of galaxies, thereby bypassing the standard cosmic distance ladder. The technique relies on X-ray observations of a cluster atmosphere and microwave measurements of the distortion by the cluster of the cosmic microwave background radiation (CMBR). In contrast to recent Cepheid-based distance determinations of galaxies, which have reached the limits of current instrumentation and still extend only to the Virgo (e.g., Pierce et al. 1994, Freedman et al. 1994) or Fornax (Madore et al. 1996) clusters, it is possible to detect (and measure) clusters in both the X-ray and SZ-effect at cosmologically interesting redshifts of ~ 1 . The only other known astrophysical techniques for distance determination that can work effectively at these distances use Type Ia supernovae (SNe) as standard candles (e.g., Hamuy et al. 1995, Riess, Press, & Kirshner 1996, Perlmutter et al. 1997) or time delay measurements of gravitational lenses (Kundić et al. 1997; Schechter et al. 1997). SNIa distances are tied to the Cepheid distance scale, since the absolute peak magnitudes of, at least, a few nearby SNe need to be calibrated, while the SZ effect and gravitational lens time delay techniques are completely independent of all rungs of the cosmic distance ladder.

The SZ effect is a distortion in the 2.7 K CMBR caused by inverse Compton scattering of the CMBR photons off electrons in the hot gas of a cluster of galaxies. This distortion appears as a decrement in the microwave background in the Rayleigh-Jeans part of the spectrum and an increment on the Wien side. Even for the richest, most massive and X-ray luminous galaxy clusters the effect is small, $\Delta I/I \sim 10^{-4}$, and thus sensitive, low noise microwave observations are required for the detection of the effect. The value of such measurements has been known for some time: comparison of the X-ray properties and the SZ effect for a cluster of galaxies may be used to measure the cluster's distance, and hence the Hubble constant (Gunn 1978, Silk & White 1978, Cavaliere, Danese, & DeZotti 1979, Birkinshaw 1979).

CL 0016+16 is one of the most distant clusters for which the SZ effect has been detected. Here we present the analysis of X-ray and Sunyaev-Zel'dovich effect data from this cluster with a fully consistent modeling of the cluster's atmosphere under the assumptions that the gas is isothermal, smooth, and follows an isothermal- β law profile (modified for the evident ellipticity of the cluster). We present a comprehensive error analysis flowing down observational uncertainties and instrumental calibration errors to the derived value of the Hubble constant. Rephaeli & Yankovitch (1997) have pointed out the importance of considering relativistic corrections to the X-ray bremsstrahlung emissivity and the CMBR spectral distortion when interpreting the SZ effect in galaxy clusters. We have corrected an error in their results for the bremsstrahlung emissivity (which derives from an earlier misprint in Gould 1980) that results in a factor of ~ 2 reduction in the magnitude of the relativistic corrections. At CL 0016+16's redshift of 0.5455 (Dressler & Gunn 1992), the effect of the cosmological parameters (Ω_0 and Λ_0) on the derived Hubble constant can be

large: of order 10%-20%, depending on the actual numerical values assumed for the parameters. We present results for a Friedmann Universe ($\Lambda_0 = 0$) with $\Omega_0 = 0.2$ (equivalently $q_0 = 0.1$) which appears to be favored by recent measurements of the mean mass density of the Universe (Carlberg et al. 1996). Correction factors are given for “adjusting” H_0 to other popular values of Ω_0 and Λ_0 .

Over the past few years, the X-ray astronomy satellite *ROSAT* has effected a profound change in our view of galaxy clusters. Its superb angular resolution and low background have allowed us to peer more closely into the morphological structure of clusters, revealing a wealth of new insights. It is clear now that clusters are complex objects, showing evidence for substructuring and dynamical activity from merging, in nearly all cases that have been examined in detail. Although a boon to astrophysicists studying the evolution of clusters, this complexity exposes a significant problem for distance determination using the SZ effect, since the technique requires knowledge of the three-dimensional distribution of electron density (and temperature) in the target galaxy cluster. We have found that new methods of analysis are necessary in order to understand and quantify the structural data. In this and future articles we investigate the effects of the complex spatial structure of galaxy clusters on the derivation of the Hubble constant from the SZ effect.

The X-ray image of the cluster CL 0016+16, in particular, shows highly significant evidence for ellipticity with a ratio of major to minor axis length of ~ 1.2 . Given this observed distribution, it is immediately obvious that an analysis based on azimuthally-averaged radial surface brightness profiles would be inadequate. We employ the more accurate, but computationally more difficult, approach of model fitting directly to the image plane. Once the projected distribution is modeled, however, the question of how to carry out the de-projection remains. In our previous work on Abell 665 (Birkinshaw, Hughes, & Arnaud 1991, hereafter BHA) and Abell 2218 (Birkinshaw & Hughes 1994), we assumed that the underlying cluster atmospheres were spherically symmetric, an approximation which cannot be good for CL 0016+16. In this article we relax the assumption of a fully spherically symmetric gas distribution and introduce the next level of geometric complexity, by taking the cluster to be an axisymmetric ellipsoidal system, with the three-dimensional isodensity contours of the cluster’s gas distribution given by concentric similar ellipsoids of revolution. For this surface brightness model the contours of constant X-ray intensity are similar concentric ellipses, and it is possible to calculate the effects of varying inclination angles on the derived value of H_0 in closed form. Since a major uncertainty in the X-ray/SZ-effect distance determination technique arises from uncertainties in the intrinsic geometry of the cluster, it is critical to examine the dependencies of derived distances on the assumptions made.

In the next section we discuss the X-ray and radio observations used. In §3 we describe the basic method of analysis for both circular and elliptical surface brightness distributions and describe the results of fits of these models to the X-ray and SZ effect data. We present the value of the Hubble constant (H_0) in §4 with a complete error analysis including both statistical and systematic errors. The effects of the unknown three-dimensional geometry

of the cluster are also presented in §4. Concluding remarks and a summary are contained in §5.

2. OBSERVATIONS

2.1. X-Ray

In order to usefully apply the method outlined above, one needs accurate measurements of the spatial distributions of density and temperature in the cluster atmosphere. The currently active satellite missions *ROSAT* (Trümper 1983) and *ASCA* (Tanaka, Inoue & Holt 1994) both provide greatly enhanced capabilities relative to previous X-ray satellites for observing these quantities for all known X-ray-emitting clusters. The various instruments among these satellites, however, are not all equally useful for determining both the density and temperature structures. Here we discuss the merits and limitations of each instrument in this regard.

The *ROSAT* Position Sensitive Proportional Counter (PSPC) (Pfeffermann et al. 1986) has good spatial resolution ($\sim 30''$ half power diameter at 1 keV), very low internal background, and a large field of view ($\sim 2^\circ$ diameter) for observations in the soft X-ray band (0.2–2.4 keV). During its lifetime (from launch in June 1990 until it ran out of detector gas four years later), this instrument revolutionized our view of the morphologies of galaxy clusters and we use it as the dataset for investigating the density structure of CL 0016+16.

The PSPC data also provide modest spectral resolution ($\Delta E/E \sim 40\%$ [FWHM] at 1 keV), which most usefully constrains the equivalent column density of absorbing neutral hydrogen along the line of sight. This quantity is essential for converting the observed rates in the detectors to the “true” X-ray flux of the cluster. The PSPC’s ability to measure the temperature of the hot intergalactic medium in rich galaxy clusters is severely limited by the upper energy cut-off of the *ROSAT* telescope which is far below the “knee” in the bremsstrahlung spectrum for $kT \sim 7$ keV. The gas temperature is therefore measured using *ASCA* data.

The Gas-Imaging Spectrometer (GIS) (Ohashi et al. 1996) on board *ASCA* can produce X-ray images of celestial sources over a broad band (0.7–10 keV) with modest spectral resolution ($E/\Delta E \sim 8\%$ [FWHM] at 6 keV). Note that there are two nominally identical detectors referred to as GIS2 and GIS3. Because of its large field of view ($\sim 40'$ diameter) and high efficiency ($>70\%$ over 1.5–10 keV), it is the instrument of choice for studying the X-ray spectra of galaxy clusters. The Solid-state Imaging Spectrometer (SIS), although it provides impressive spectral resolution, is considerably less efficient than the GIS at detecting harder X-ray photons ($E \gtrsim 4$ keV). This makes the SIS less accurate than the GIS for temperature determination. Indeed an earlier analysis of *ASCA* data on CL 0016+16 (Yamashita 1994) showed that the uncertainty in the mean temperature from the SIS data was 6–10 times larger than the uncertainty from the GIS. (The best fit values were statistically consistent.) In our spectral analysis we concentrate on joint spectral fits of the low energy PSPC data with the higher energy GIS data.

On the other hand, the limited spatial resolution of the *ASCA* X-ray telescope (half-power diameter of $\sim 3'$), which is further broadened by the position resolution of the GIS ($\sim 0.5'$ at 6 keV) makes this data considerably less useful than the PSPC data for determining the detailed internal structure of clusters. It also means that measurement of the spatial distribution of temperature remains impossible for such a distant cluster with current instrumentation.

2.1.1. *ROSAT* PSPC Imaging

We observed CL 0016+16 with the PSPC in 1992 July for an effective live-time corrected exposure time of 43,157 s. The observation was carried out in the standard wobbled mode. Figure 1 shows a central portion of the field. The grayscale presents the number of raw detected events over the 0.4-2.4 keV band in $7''5$ square pixels. The contours show the same data after background subtraction and exposure correction (using the standard files supplied as part of the *ROSAT* standard processing) and smoothing with an intensity-dependent smoothing kernel. This smoothing employed a Gaussian function with standard deviation increasing from $7''5$ in the brightest parts of the image to $1'$ in the dimmest.

The cluster appears as the clearly extended source near the center of Figure 1. At its peak near the center, CL 0016+16 is a factor of 100 times brighter than the mean background level. The intensity of the cluster is roughly equal to the background level at a radius of $\sim 3'$ (1.3 Mpc). Only a few of the numerous serendipitous sources that appear in the field have been identified; we mention some of them below. In our spatial analysis, and when spectra are extracted for either source or background regions, we exclude circular regions of radius $52''$ centered on these sources. For three relatively bright sources (one of which is the unresolved source north of the cluster), we use a circular radius of $80''$ for the exclusion region.

We verified that the standard background file provided an acceptable fit to the data using our image fitting software (see below). We scaled the background image by a multiplicative factor to fit the data in an annular region covering $5'$ – $10'$ centered on the cluster, excluding all sources detected by the standard processing, but including the small contribution in this region from the X-ray emission of CL 0016+16 itself, based on the model fits determined using the nominal (i.e., unit scaled) background. The multiplicative factor obtained is $97\% \pm 3\%$. Over the region of interest, i.e., the central $10'$ of the detector, the variation in background, as well as the vignetting correction, was small, $<5\%$.

The PSPC data were boresight corrected using the optical or radio positions of 5 sources that were coincident with unresolved X-ray sources. Among these were 3 *HST* guide stars at positions (all positions are quoted in epoch J2000 throughout this paper) $00^{\text{h}}17^{\text{m}}22.1^{\text{s}}$, $16^{\circ}30'35''$; $00^{\text{h}}17^{\text{m}}59.1^{\text{s}}$, $16^{\circ}40'22''$; and $00^{\text{h}}19^{\text{m}}11.9^{\text{s}}$, $16^{\circ}18'53''$. These sources all lie outside the field of view shown in Figure 1. We also used QSO 0015+162 at position $00^{\text{h}}18^{\text{m}}31.9^{\text{s}}$, $16^{\circ}29'26''$, which has a redshift $z = 0.554 \pm 0.002$ that is very nearly the same as CL 0016+16 (Margon, Downes, & Spinrad 1983). This source is the bright point source $3'3$ north of the cluster in Figure 1; we will be discussing it in some more detail later. The unidentified radio source number 15 in the Moffett & Birkinshaw

(1989) VLA survey of CL 0016+16 (at position $00^{\text{h}}18^{\text{m}}31.3^{\text{s}}$, $16^{\circ}20'43''$) also appeared as a PSPC X-ray source and can be located in Figure 1. The X-ray source positions were taken from the standard processing and compared to the “true” (i.e., optical or radio) source positions. There was a difference of 0.28 ± 0.18 s in right ascension and 7.3 ± 2.1 arcseconds in declination with the X-ray positions being east and north of the true positions. This corresponds to an error in absolute position reconstruction of $8''.3$, which is within the usual range for PSPC data. In the following, we quote boresight-corrected X-ray positions.

2.1.2. *ROSAT* PSPC Spectroscopy

The light curve (count rate versus time) of the entire PSPC field shows large count rate excursions (up to factors of two) for short time periods near the beginning and end of most of the good-time-intervals provided with the *ROSAT* standard processing. These flares are mostly in the 0.4–0.8 keV band and we attribute them to solar X-ray fluorescent emission of atmospheric nitrogen and oxygen from the bright limb of the earth. We cleaned the data of this contamination by eliminating the time intervals of high background, thereby reducing the effective live time of the observation, for spectral studies only, to 38109.0 s.

The cluster spectrum was extracted from within a circular region of radius $200''$ centered on the location of the peak cluster brightness and the background came from a concentric annulus with inner and outer radii $300''$ and $500''$. All sources (other than the cluster) were excluded from both source and background regions. We also extracted a spectrum of the AGN, QSO 0015+162, from a circular region of radius $80''$, employing the same annular background region. Figure 2 shows the spectrum of each of these two sources. The observed PSPC count rate of CL 0016+16 (after background subtraction) is $(8.57 \pm 0.17) \times 10^{-2} \text{ s}^{-1}$, while that of QSO 0015+162 is $(1.20 \pm 0.08) \times 10^{-2} \text{ s}^{-1}$. The background counting rates associated with these sources are 0.016 s^{-1} and 0.003 s^{-1} , respectively.

2.1.3. *ASCA* GIS Spectroscopy

The GIS observed CL 0016+16 in mid July, 1993, during the Performance Verification phase of the *ASCA* mission, for an effective exposure time ~ 35000 s. We extracted the data from the *ASCA* archive at the HEASARC and employed standard screening criteria to the data: avoidance of South Atlantic Anomaly passages, geomagnetic cosmic ray cut-off rigidity $> 6 \text{ GeV}/c$, and elevation angle between the pointing direction and limb of the Earth $> 10^{\circ}$. The light curve of the entire field of view was examined and no rate anomalies were noted. Background was taken from the high Galactic latitude blank sky observations available from the *ASCA* Guest Observer Facility with screening criteria matched to be the same as those used for the CL 0016+16 data. For both source and background fields, rise time information (in the form of the RTI, or rise-time invariant, values) was used to reject charged particle (i.e., non-X-ray) events.

In the GIS image the cluster appeared as a slightly extended source. However, due to its limited angular resolution, only a few serendipitous sources were obvious in the GIS map and, more importantly, the X-ray source QSO 0015+162 was not cleanly resolved from the cluster. We extracted the spectrum from within a circular region of radius $5'$

which included emission from both the cluster and the AGN. The position and size of this region were chosen to avoid a couple of background sources toward the south of the cluster. Background came from the same region in detector coordinates as the source. The GIS spectrum is displayed in Figure 2. The background subtracted counting rate of CL 0016+16 (the average of GIS2 and GIS3) was $(4.64 \pm 0.13) \times 10^{-2} \text{ s}^{-1}$. The background rate was 0.013 s^{-1} .

2.2. OVRO Sunyaev-Zel'dovich Effect Data

The Sunyaev-Zel'dovich effect for CL 0016+16 was measured using the 40-m telescope of the Owens Valley Radio Observatory (OVRO) at 20.3 GHz over the period 1983-1990 (Birkinshaw et al. 1997). The method used was similar to that used to measure the SZ effects of Abell 665 and 2218. The dual-beam system on the 40-m telescope provides two 1.78-arcmin FWHM beams separated by 7.15 arcmin in azimuth. Data were taken using beam-switching and position-switching at seven locations on a north-south line through the center of CL 0016+16 (as determined from *Einstein Observatory* data). The measured SZ effect signals therefore represent the difference between the brightness of the microwave background radiation towards the scan locations and a weighed average of points in “reference arcs” centered 7.15 arcmin from them. These reference arcs are irregularly sampled because of the varying rate with which the parallactic angle of the reference beams changes with time, because of the exclusion of some parts of the reference arcs because of radio source contamination, and because of the varying weather conditions over the observations. This irregular sampling causes the measured SZ effects to be complicated functions of the intrinsic SZ effect of CL 0016+16.

Figure 3 shows the measurements at these seven locations in CL 0016+16, after averaging the best data taken over the entire observing period and correcting for the presence of contaminating radio sources. The largest radio-source corrections were needed at the points 4 and 7 arcminutes south of the center of the cluster: the errors on the measurements at these points are large because of the uncertainty in the corrections. Fortunately, these heavily-contaminated points lie sufficiently far from the center of CL 0016+16 that the source corrections have little effect on the fitted amplitude of the cluster SZ effect.

In addition to the statistical errors, the error bars shown in Fig. 3 contain contributions from the year-to-year inconsistency in the data, uncertainties in the radio source corrections, and errors in the telescope pointing. These are significant for the points 7 and 4 arcmin south of the cluster center (near a bright radio source), but make only small corrections to the errors elsewhere. A further systematic error represented in Fig. 3 is the possible offset in the zero level of the data, such as might be caused by differential spillover effects (see Birkinshaw et al. 1997). This zero level offset is best measured by the amount that extreme points in the scan are offset from the nominal zero level, after correction for the expected SZ effects at the outer points. For CL 0016+16 the best-fit zero level offset is $+70 \pm 43 \mu\text{K}$, reflecting the tendency of the outer points in the scan to lie at positive brightness temperatures. The range of this zero level error is represented by the horizontal lines in Fig. 3.

A final important source of uncertainty is that arising from the brightness temperature scale. This was based on an internal noise source in the receiver, which was independently calibrated using hot and cold loads, planets, and measurements of unresolved radio sources. An absolute error of 6% arises from uncertainty in the beam response of the telescope, while the calibrated value of the equivalent brightness of the internal load has a 5% error. Combining these errors together, the overall systematic uncertainty in the brightness temperature scale in Fig. 3 may be as much as 8%.

It can be seen that CL 0016+16 shows a strong central SZ effect, and that this SZ effect is extended by more than the 1.78-arcmin FWHM beam of the 40-m telescope. The measured SZ effect near the center of the cluster is $-490 \pm 80 \mu\text{K}$ (with no zero level offset), about half the intrinsic SZ effect of the cluster.

3. ANALYSIS

3.1. Basic Method

BHA derived the following generalized expressions for the X-ray surface brightness and the Sunyaev-Zel'dovich effect from a cluster of galaxies

$$b_X(\theta, \phi) = \frac{1}{4\pi(1+z)^3} \Lambda_{e0} n_{e0}^2 D_A \int d\zeta f_n^2 f_\Lambda \quad (1)$$

$$\equiv N_X \Theta_X$$

$$\Delta T_{RJ}(\theta, \phi) = -2T_r \frac{k_B T_{e0}}{m_e c^2} \sigma_T n_{e0} D_A \int d\zeta f_n f_T \quad (2)$$

$$\equiv N_{RJ} \Theta_{RJ} ,$$

where θ and ϕ form a Cartesian coordinate system. In these equations T_r ($= 2.728 \text{ K}$, Fixsen et al. 1996) is the temperature of the microwave background radiation, z ($= 0.5455$) is the cluster redshift, Λ_{e0} is the spectral emissivity of the cluster gas at T_{e0} calculated over the emitted energy range appropriate for the observed energy range of 0.4–2.4 keV, n_{e0} is the electron number density at the center of the cluster, T_{e0} is the central electron temperature, D_A is the angular diameter distance of the cluster, σ_T is the Thomson scattering cross-section, k_B is the Boltzmann constant, m_e is the electron mass, and c is the speed of light. The variation of the electron density, temperature, and the spectral emissivity with (three-dimensional) position in the cluster is contained in the dimensionless form factors f_n , f_T , and f_Λ . ζ is an angular measure of distance along the line of sight. The structural information on the cluster is contained in the angles Θ_X and Θ_{RJ} and the normalizations of the X-ray and SZ effects are in N_X and N_{RJ} .

Our previous work (BHA; Birkinshaw & Hughes 1994) considered only spherical cluster atmospheres. Here we extend the analysis to include elliptical models. For convenience we first present a summary of the analysis using circular isothermal- β models to describe the gas distribution before proceeding to the more general cases.

3.1.1. Circular Isothermal- β Model

Under the assumption of an isothermal atmosphere ($f_T = 1$, $f_\Lambda = 1$), with a density distribution given by $n_e = n_{e0}[1 + (r/r_c)^2]^{-3\beta/2}$ (Cavaliere & Fusco-Femiano 1976, 1978) we derive

$$\Theta_X(\theta, \phi) = \sqrt{\pi} \frac{\Gamma(3\beta - \frac{1}{2})}{\Gamma(3\beta)} \theta_C \left(1 + \frac{\theta^2 + \phi^2}{\theta_C^2}\right)^{\frac{1}{2} - 3\beta} \quad (3)$$

$$\Theta_{RJ}(\theta, \phi) = \sqrt{\pi} \frac{\Gamma(\frac{3\beta}{2} - \frac{1}{2})}{\Gamma(\frac{3\beta}{2})} \theta_C \left(1 + \frac{\theta^2 + \phi^2}{\theta_C^2}\right)^{\frac{1}{2} - \frac{3\beta}{2}} \quad (4)$$

for the forms of the X-ray and SZ surface brightnesses of the cluster. The angular diameter distance of the cluster is given by

$$D_A = \left(\frac{N_{RJ}^2}{N_X}\right) \left(\frac{m_e c^2}{k_B T_{e0}}\right)^2 \frac{\Lambda_{e0}}{16\pi T_r^2 \sigma_T^2 (1+z)^3}. \quad (5)$$

In practice, we analyze the PSPC X-ray image to determine best-fit values and errors for the quantities β , θ_C , and N_X . These values are used to construct model SZ profiles (including the appropriate subtraction of residual cluster emission in the reference arcs) which are then fit to the OVRO scan data to obtain N_{RJ} . We make the assumption that the cluster atmosphere is isothermal, i.e., the form factors f_T and f_Λ are everywhere equal to unity. Thus the remaining observable quantity, $k_B T_{e0}$, can be obtained from *ASCA* X-ray spectroscopy.

3.1.2. Elliptical Isothermal- β Model

In this case, the surface brightness of the cluster is assumed to be a function of $[\theta^2 + (e\phi)^2]/\theta_C^2$, where θ lies along the major axis of the cluster, ϕ along the minor axis, and e is the ratio of major to minor axes. We assume that the three dimensional structure of the cluster is given by an ellipsoid of revolution with the symmetry axis lying at inclination angle i to the line of sight (see Fabricant, Rybicki, & Gorenstein 1984 for details on the projection of spheroids). The results then depend on whether we assume an oblate (with the symmetry axis lying along ϕ) or prolate (symmetry axis along θ) geometry. Again an isothermal atmosphere is assumed.

For an oblate geometry we find

$$\Theta_X(\theta, \phi) = \sqrt{\pi} \frac{\Gamma(3\beta - \frac{1}{2})}{\Gamma(3\beta)} \theta_C \frac{\sqrt{1 - e^2 \cos^2 i}}{\sin i} \left(1 + \frac{\theta^2 + (e\phi)^2}{\theta_C^2}\right)^{\frac{1}{2} - 3\beta} \quad (6)$$

$$\Theta_{RJ}(\theta, \phi) = \sqrt{\pi} \frac{\Gamma(\frac{3\beta}{2} - \frac{1}{2})}{\Gamma(\frac{3\beta}{2})} \theta_C \frac{\sqrt{1 - e^2 \cos^2 i}}{\sin i} \left(1 + \frac{\theta^2 + (e\phi)^2}{\theta_C^2}\right)^{\frac{1}{2} - \frac{3\beta}{2}} \quad (7)$$

while a prolate geometry yields

$$\Theta_X(\theta, \phi) = \sqrt{\pi} \frac{\Gamma(3\beta - \frac{1}{2})}{\Gamma(3\beta)} \theta_C \frac{\sqrt{e^2 - \cos^2 i}}{e^2 \sin i} \left(1 + \frac{\theta^2 + (e\phi)^2}{\theta_C^2}\right)^{\frac{1}{2} - 3\beta} \quad (8)$$

$$\Theta_{RJ}(\theta, \phi) = \sqrt{\pi} \frac{\Gamma(\frac{3\beta}{2} - \frac{1}{2})}{\Gamma(\frac{3\beta}{2})} \theta_C \frac{\sqrt{e^2 - \cos^2 i}}{e^2 \sin i} \left(1 + \frac{\theta^2 + (e\phi)^2}{\theta_C^2}\right)^{\frac{1}{2} - \frac{3\beta}{2}}. \quad (9)$$

The equation for D_A is the same as above (eqn. 5). Here the X-ray image provides values and errors for the quantities β , θ_C , e , the position angle of the major axis, and N_X while fits to the SZ data yield N_{RJ} . We present results for different assumed inclination angles and for the oblate and prolate geometries.

3.2. Fits to the X-ray image

The purpose of our image analysis is to explore fits of the preceding classes of structural models to the CL 0016+16 X-ray data in order to produce an accurate representation of the density structure of the cluster. In addition to determining best-fit values and errors for the relevant parameters we also would like to determine the goodness-of-fit of these models. The standard method of fitting an azimuthally averaged radial surface brightness profile, as has been applied most widely to cluster data in the past, is grossly inadequate to explore the complex structures that now, thanks to *ROSAT*, are clearly evident in the image of CL 0016+16 and other clusters. The approach we take here is one that we introduced earlier (BHA, Birkinshaw & Hughes 1994) and is based on performing spatial model fits directly to the two-dimensional image data. This approach provides us with the flexibility to explore the complex structures necessary to understand fully the morphologies of galaxy clusters.

X-ray images of clusters are sparsely filled with most image pixels containing zero or one detected event and CL 0016+16 is no exception (the mean number of events per pixel of the image shown in Figure 1 is ~ 1). The statistical error associated with counting experiments of this kind follow a Poisson distribution. Only in the case of a large enough number of detected events (typically $\gtrsim 10$) does a Gaussian distribution serve as an adequate approximation to the Poisson distribution. Since the usual figure-of-merit function, the χ^2 statistic, requires that measurement errors be normally distributed, we were led to derive a different maximum likelihood estimator for the Poisson distributed error case.

The Poisson probability that D_{ij} events were observed in a given image pixel, (i, j) , for a predicted number of model X-ray events M_{ij} is $P_{ij} = M_{ij}^{D_{ij}} e^{-M_{ij}} / D_{ij}!$. The likelihood function L is the product of the individual probabilities P_{ij} over all pixels in the region of the image being fitted. For reasons having to do with determining confidence intervals (as discussed below), we choose to minimize the function $S \equiv -2 \ln L$ which is equivalent to maximizing L . Thus our figure-of-merit function becomes

$$S = \sum_{ij} 2M_{ij} - 2D_{ij} \ln M_{ij}, \quad (10)$$

where we have dropped all terms that do not depend on the model being fitted. We employ the robust downhill simplex method (Press et al. 1986) for function minimization.

This new estimator, however, does not provide an analytic goodness-of-fit criterion. In our work here, we take the following approach. Radial profiles about the cluster center of the X-ray data and best-fit model in four azimuthal sectors (defined by the ordinal compass directions) are compared in a χ^2 test and only radial bins containing more than 10 events are used in the calculation. In the results presented below, we give the χ^2 values computed in this manner for the various structural models.

On the other hand, our function S does provide a method for determining the relative goodness-of-fit between different models and for the estimation of confidence intervals, through the “likelihood ratio test.” This test is carried out by comparing the value S_{\min} , determined by minimizing the figure-of-merit function over all relevant parameters, with the value S_r , which is determined from a fit where r parameters have values that differ from the best fit ones. It can be shown that the distribution function of $S_r - S_{\min}$ tends to a χ^2 distribution with r degrees of freedom (see, for example, Kendall & Stuart 1979).

As mentioned earlier, circular regions centered on all non-cluster X-ray sources were excluded from the fits; these image pixels were not used in the computation of the likelihood function. Aside from this, the fit included all pixels within a $5'$ radius of the peak cluster emission. All results are quoted below for the same fixed region. We did explore the effect of fitting the data over a smaller region in radius ($3'$) and found that the change in derived parameter values was negligible. Our model included exposure correction and convolution (in the Fourier domain) with the on-axis PSPC point response function (Hasinger et al. 1992) calculated for a photon energy of 1 keV. This is important, but its effect is not overwhelming: the FWHM of the *ROSAT* PSPC point response function is $\sim 25''$, which is about $1/4$ of the FWHM of the cluster itself.

Fits were carried out first to the circular isothermal- β model. Numerical values of the best-fit parameters are given in Table 1. The position of the center of the X-ray cluster is consistent (agrees to within $<10''$) with the position of the central bright galaxy in the cluster (Dressler & Gunn 1992). The best-fit θ_C value corresponds to a reasonable physical size of ~ 340 kpc at the cluster (for $H_0 = 50 \text{ km s}^{-1} \text{ Mpc}^{-1}$, $q_0 = 0.1$). However, this fit is not particularly good. The χ^2 (for the data and model binned in quadrants) of 140.1 for 91 degrees of freedom can be formally rejected at the 99.93% confidence level. The error intervals presented in the last column of the table are based on the likelihood ratio test. The value of 1.0 used for $S_r - S_{\min}$ corresponds to the $1\text{-}\sigma$ confidence level for a single interesting parameter ($r = 1$).

As clearly suggested by the imaging data, a considerably better fit is provided by the elliptical isothermal- β model. The best-fit elliptical model yields a value of S_{\min} that is less than the best-fit circular case by 35.5. This is a highly significant reduction in S for the introduction of two additional parameters and corresponds to a confidence level of greater than 5σ for the rejection of the circular model relative to the elliptical one. Our estimate of the absolute goodness-of-fit also indicates that this model is a better fit than

the previous one, but even this improved χ^2 of 117.5 can be formally rejected at about the 96.8% confidence level. Fitted parameters and errors for the elliptical model are shown in Table 2. The center of the cluster is nearly unchanged from the location fitted based on a spherical model. The cluster’s ellipticity is quoted in terms of the ratio of major to minor axis length, e , which appears in equations 6–9. The position angle of the major axis is measured east of north. Figure 4a shows the radial profiles of the model and data azimuthally averaged over quadrants and figure 4b shows the residuals. We note that our numerical results are consistent with those of Neumann & Böhringer (1997).²

3.3. Fits to the Sunyaev-Zel’dovich effect data

The SZ effect data considerably undersample the structure of the cluster (only a single north-south scan through CL 0016+16 is available), and thus cannot provide useful constraints on the model of the cluster gas. For this reason we use the SZ effect data only to determine the normalization of the SZ effect by fitting with structural models consistent with the X-ray imaging. In the error analysis we were careful to include correlations among parameters; in particular θ_C , β , and the X-ray and SZ-effect normalizations are highly correlated.

Using the parameters of the best-fit circular isothermal- β model (Table 1) we find a central SZ decrement of $\Delta T_{RJ}(0) = -1.20 \pm 0.19$ mK. This value includes the zero-level offset of $+70 \pm 43$ μ K (as quoted in Sec. 2.2) and the error includes a contribution from the uncertainty in the zero-level. The χ^2 associated with this fit is not particularly good, $\chi^2 = 10.5$ for 5 degrees of freedom, since the SZ effect data appear to be consistent with a somewhat flatter central gas density distribution than the X-ray data. The central SZ decrement in the absence of a zero-level correction is smaller and corresponds to a central SZ decrement of $\Delta T_{RJ}(0) \approx -1.0$ mK. This fit is somewhat worse: $\chi^2 = 13.0$ for 6 degrees of freedom. The effect of the zero-level offset is the largest systematic error in the Sunyaev-Zel’dovich effect normalization and is particularly pernicious because it is a one-sided error, and may therefore introduce a bias in the result for H_0 .

For the elliptical isothermal- β model (Table 2) fits to the SZ effect data result in nearly identical values for the central SZ decrement $\Delta T_{RJ}(0) = -1.21 \pm 0.19$ mK, with a similar goodness of fit to that for the circular model: $\chi^2 = 10.8$ for 5 degrees of freedom.

3.4. Fits to the X-ray spectra

² We take this opportunity to correct a statement by these authors identifying a disadvantage to our use of maximum likelihood fits for X-ray images (near the end of §3.2 of their paper). In fact, our maximum likelihood fits have always allowed for the determination of best-fit parameter values (and confidence intervals) by locating the minimum of the figure-of-merit function, S . Furthermore since our method is based on using the appropriate Poisson distribution for the raw data, rather than applying Gaussian filters to the data and assigning arbitrary error values to blank pixels (as Neumann & Böhringer do) it should result in more robust parameter values and confidence intervals.

Our spectral fits are driven by two principal goals: (1) determination of the mean temperature of the hot electrons, kT_e , in the plasma of the intracluster medium, and (2) determination of the spectral emissivity, Λ_e , of the gas as observed by the PSPC. The temperature is determined mainly by constraining the shape of the X-ray continuum emission in the *ASCA* data. The spectral emissivity is calculated from a standard thermal plasma code (we use the model of Raymond & Smith 1977; 1992 July 27 version) and depends on kT_{e0} , the metallicity of the gas, and the column density of neutral hydrogen (N_{H}) along the line of sight which causes absorption of soft X-rays from the cluster. This latter quantity is most usefully determined from the PSPC spectral data. Clearly, therefore, a joint spectral fit of the GIS and PSPC data will provide the most accurate constraints on the relevant spectral parameters, leading in turn to the most accurate values possible for the quantities of interest.

The spectral fits were complicated in part by the X-ray emission from QSO 0015+162 since this is not separated from the cluster emission by the GIS. The approach we took was to extract independent PSPC spectra of QSO 0015+162 and CL 0016+16, and to fit appropriate spectral models to each: a power-law for the AGN and a thermal plasma model for the cluster. The sum of these models was required to fit the GIS data. In total the spectral fits involved six free parameters: the temperature and iron abundance of the cluster gas, the power-law index of the AGN, the absorbing column density due to gas in our Galaxy (the same value was used for both objects), and normalizations for both spectra. The redshift of the cluster was fixed to the optically derived value, $z = 0.5455$.

The joint fit of the three datasets to the two spectral models is formally acceptable with a minimum χ^2 of 220.9 for 230 degrees of freedom. Figure 2 shows the data, best fit models and residuals. Table 3 presents numerical values for the fitted quantities. The cluster temperature corresponds to the value in the source-frame. Our values for kT and iron abundance are consistent, within the errors, with those quoted earlier by Yamashita (1994). Note that the best-fit column density 5.6×10^{20} atoms cm^{-2} is only slightly higher than the Galactic value of 4.1×10^{20} atoms cm^{-2} (Stark et al. 1984). We define the emission measure of the cluster in terms of the luminosity distance D_L and the integral of the electron and proton densities, n_e and n_p , over the cluster volume V as $\int n_e n_p dV / (4\pi D_L^2)$. The photon index of the AGN power-law model, $dN/dE \sim E^{-\alpha_p}$ indicates a rather steep spectrum that does not contribute greatly to the total X-ray emission in the GIS 2–10 keV band.

We also investigated the sensitivity of the derived temperature to uncertainty in background subtraction for the GIS data. Varying the normalization of the background by $\pm 6\%$ of the nominal value had the effect of changing the best fit temperature by ${}_{+0.35}^{-0.33}$ keV. These errors are included in the results of Table 3 (see footnote), but are only about half the size of the statistical errors.

3.5. *Relativistic Corrections to X-ray Bremsstrahlung Emissivity*

Use of the Sunyaev-Zel'dovich effect for distance determination to galaxy clusters is based on our ability to calculate from fundamental physics accurate expressions for the

spectral intensity of X-ray bremsstrahlung emission and the inverse Compton scattering distortions to the CMBR. In most analyses to date nonrelativistic approximations have been employed for these expressions. For example the Raymond & Smith code mentioned above uses the Gaunt factor evaluated by Karzas & Latter (1961) in the nonrelativistic limit for the bremsstrahlung component of the plasma emission. Recently Rephaeli & Yankovitch (1997) have pointed out the importance of including relativistic corrections (i.e., first order in kT_e/mc^2) for accurate work in determining H_0 from rich galaxy clusters where kT_e can be as large as 15 keV. In the following we employ their expressions for the relativistic corrections to the intensity change of the CMBR (which agree with other calculations, e.g., Birkinshaw 1998), but have found an error in their relativistic X-ray bremsstrahlung emissivity which we detail below.

Although we refer to these as “relativistic” corrections, in fact, the results that we and Rephaeli & Yankovitch both use for X-ray bremsstrahlung come from Gould (1980). These calculations use the nonrelativistic Born approximation as the principle term for the electron-ion bremsstrahlung cross section and then include first-order corrections from relativistic effects (both to the thermal electron velocity distribution function and the electron-ion bremsstrahlung cross section), emission from electron-electron bremsstrahlung, and a first order correction to the Born approximation, which is most important at lower temperatures. These modifications are each of order 10% and, when applied, are expected to result in a formula for thermal bremsstrahlung emission that is accurate to 1% for a ~ 10 keV plasma. Gould (1980) presents results for both the total energy-loss rate (integrated over frequency) and the spectral emissivity of thermal bremsstrahlung.

Rephaeli & Yankovitch start from Gould’s formula for the total energy-loss rate which they note is significantly larger than expressions for relativistic corrections to bremsstrahlung published in standard texts (e.g., Rybicki & Lightman 1979). We have identified a misprint³ in Gould (1980) that accounts for most of this difference. However, considering this issue further we find that we disagree with the use of the integrated bremsstrahlung energy-loss rate since what matters is the effects of the relativistic corrections on (1) the calculated value of Λ_e , which, as discussed above, comes from integrating the thermal bremsstrahlung emissivity function over the, relatively narrow, redshifted *ROSAT* energy band, and (2) the fitted value of kT_e from X-ray spectra. Addressing both of these issues requires use of the spectral emissivity formula and so this is what we have chosen to implement. As a check we have verified that the Gould’s spectral emissivity formula (eqn. 43), when integrated over frequency, agrees with the (corrected) total energy-loss rate formula.

Rephaeli & Yankovitch argue that the effect of relativistic corrections on the fitted value of kT_e should be small since it is the exponential factor that dominates the shape of a bremsstrahlung spectrum and hence drives the spectral fits. Work we have done confirms that suspicion. In the course of analyzing the *Ginga* spectrum of the Coma cluster (Hughes et al. 1993), which covered the 2–20 keV band, we used both the Karzas & Latter (1961)

³ In the brackets in equation 41 of Gould (1980), the value 8 in the denominator of the second term should be replaced with the value 24. This follows directly from equation 22.

and Gould (1980) calculations to derive the cluster temperature. The kT_e values obtained: 8.07 ± 0.09 and 7.96 ± 0.09 , respectively, differ by only $\sim 1\%$, and clearly establish that the inclusion of relativistic corrections to X-ray bremsstrahlung emissivity do not significantly change fitted temperature values.

As for the numerical value of Λ_e , we used the results in Table 3 to calculate the spectral emissivity of the hot plasma in CL 0016+16 over the identical PSPC X-ray band used for the imaging analysis. For the best-fit spectral values and including relativistic corrections we find $\Lambda_e = 2.88 \times 10^{-13}$ PSPC ct s $^{-1}$ cm $^{-5}$. (Note that this relativistically-corrected value for Λ_e is only 1.048 times larger than the nonrelativistic value.) The variation of Λ_e is less than 2.5% over the entire range of parameter values bounded by the errors quoted in Table 3.

4. THE VALUE OF THE HUBBLE CONSTANT

4.1. Effect of Different Cosmologies

In our previous work on the relatively nearby clusters Abell 665 (BHA) and Abell 2218 (Birkinshaw & Hughes 1994) we presented values of H_0 assuming a Friedmann cosmology and a value of 0 for the deceleration parameter, q_0 . At the redshifts of these clusters ($z \sim 0.17 - 0.18$), the dependence of H_0 on the values of the other cosmological parameters is not strong. For example, the assumption of an Einstein-de Sitter universe ($q_0 = 0.5$) would have changed our derived values of H_0 by merely 3%. The situation is different for the more distant cluster CL 0016+16, where distance estimates depend significantly not only on the mean density of the universe, but on the value of the cosmological constant (Kobayashi, Sasaki, & Suto 1996).

Although our results for CL 0016+16 are not accurate enough to place significant observational constraints on the density of the universe or the cosmological constant, we nonetheless wish to present our results in the context of the currently reasonable range of acceptable cosmologies. To this end we write our equation for H_0 as

$$H_0 = \frac{cz}{D_A} \frac{1+z/2}{(1+z)^2} f(z, \Omega_0, \lambda_0), \quad (11)$$

where $f(z, \Omega_0, \lambda_0)$ contains all the functional dependence on the density parameter Ω_0 and the dimensionless cosmological constant λ_0 . Our definition of f is such that for $\Omega_0 = 0$ and $\lambda_0 = 0$, $f = 1$. In the case of Friedmann universes (i.e., $\lambda_0 = 0$), f has an analytical closed form expression (see equation 15.3.24 in Weinberg 1972), although in the more general case with a non-vanishing cosmological constant an integral over redshift must be carried out (see Carroll, Press, & Turner 1992). In Figure 5 we present curves of f versus z for several representative values of Ω_0 and λ_0 . The two extreme curves correspond to flat universes where $\Omega_0 + \lambda_0 = 1$, as favored by inflationary models of the early Universe.

In the following we quote H_0 values for CL 0016+16 assuming $\Omega_0 = 0.2$, $\lambda_0 = 0$, for which $f = 0.97$ at the cluster's redshift ($z = 0.5455$). For the curves shown in Fig. 5 f varies from 0.87 to 1.10 at the same redshift.

4.2. Basic Error Analysis

The value of the Hubble constant derived for the best-fit circular isothermal- β model (Table 1) using the best-fit spectral parameters (Table 3) is $47.2 \text{ km s}^{-1} \text{ Mpc}^{-1}$. The error budget is presented in Table 4 (values are at the 68.3%, or 1σ , confidence level). The errors are dominated by the measurements of temperature and the SZ-effect normalization. Uncertainty in metallicity and column density enter into the error budget only through their effect on Λ_e . Although the uncertainty in the metallicity of the gas is large, at the relatively high temperature of the cluster there is little emission from metals in the *ROSAT* band and so the variation in Λ_e is small. The variation in Λ_e due to the error range in column density is also small: the calculated X-ray absorption at an energy of 1 keV varies by only about $\pm 1\%$ over the allowed range of N_{H} . Note that only a single value is presented for the uncertainty in H_0 due to the structural parameters of the circular model ($b_X(0)$, β , and θ_C). Since these parameter values are correlated, as mentioned above, we determined their effect by calculating trial values of H_0 over the three-dimensional 68.3% confidence level error surface (specifically for $S - S_{\text{min}} = 3.53$). Clearly the error due to statistical uncertainty in the parameter values associated with fits to this particular model are quite small. However, as we see below, these errors are entirely dominated by the uncertainties in deprojection of the elliptical model fits.

In addition to the quantities shown in Table 4 we also have investigated systematic errors due to overall flux or brightness temperature calibration uncertainties. The absolute flux of the cluster is probably uncertain by $\pm 10\%$ due to residual uncertainties in the overall effective area calibration of *ROSAT*, which results in an uncertainty in H_0 of $\pm 4.7 \text{ km s}^{-1} \text{ Mpc}^{-1}$. Likewise, the overall SZ-effect normalization, $\Delta T_{RJ}(0)$ is uncertain by $\pm 8\%$ due to uncertainty in the efficiency of the 40-m telescope for an error in H_0 of ${}_{+8.5}^{-6.8} \text{ km s}^{-1} \text{ Mpc}^{-1}$. Combining all the errors in quadrature we obtain

$$H_0 = 47_{-16}^{+23} \text{ km s}^{-1} \text{ Mpc}^{-1}. \quad (12)$$

If the effect of a zero-level offset to the SZ-effect data ($+70 \mu\text{K}$) were not included in result (12), the derived value would be increased by $21 \text{ km s}^{-1} \text{ Mpc}^{-1}$.

The breakdown of errors in Table 4 indicate where improvement of the observations should be focussed. Clearly a longer observation with *ASCA* to reduce the statistical error in temperature would be extremely valuable. Indeed a long follow-up observation of CL 0016+16 by *ASCA* was carried out last year but the data are not generally available yet. The other major, and in fact dominant, source of error is in the SZ-effect normalization which also enters quadratically in eqn. 5. Interferometric observations of the SZ-effect from CL 0016+16 and other clusters have been reported recently (Carlstrom, Joy, & Grego 1996). These data are significantly less susceptible to errors from zero-level offsets and are of considerably higher sensitivity as compared to the data from the 40-m telescope, which in combination should greatly reduce the overall errors on H_0 . In a future article we will be comparing our models for the cluster atmosphere to these interferometric SZ-effect data to derive a more precise value of the Hubble constant.

4.3. *Effects of Unknown Geometry*

The accuracy in any measurement of H_0 from a single cluster, however, is ultimately limited by uncertainties in the unknown three-dimensional geometry of the target cluster. For example, the isothermal- β model we use in our analysis is unbounded, i.e., the gas distribution extends to infinite radial extent. Although this is clearly an approximation to the situation of a real cluster, it turns out to be a rather good one. In cases that have been well-observed, like the Coma Cluster (Briel, Henry, & Böhringer 1992), the isothermal- β model provides an excellent description of the X-ray surface brightness profile out to roughly 10 core radii. Nevertheless it is important to consider the effect that a radial truncation in the cluster gas distribution might introduce in the determination of H_0 for any particular cluster.

The radially averaged X-ray surface brightness of CL 0016+16 can be confidently traced to approximately $5'$, or roughly $7\theta_C$, where the cluster emission is $\sim 25\%$ of the local background rate. We implement a truncated model by modifying the isothermal- β model form factor f_n used to derive equations (3) and (4) so that $f_n = 0$ for $r > r_{\max}$. Using the truncation radius determined from the cluster's maximum angular extent, we fit for new values of N_X , β , and θ_C from the X-ray image and for a new value of N_{RJ} from the SZ effect scan data (using the new best-fit β and θ_C values), assuming a circular isothermal- β model. The best fit values of $\beta = 0.69$ and $\theta_C = 0'.64$ are somewhat smaller (and the quality of the fit is worse) than the untruncated model. Carrying the new normalization factors through to a value for the Hubble constant we find $H_0 = 50.2 \text{ km s}^{-1} \text{ Mpc}^{-1}$, some 6% higher than our best estimate based on the untruncated model. This difference is given by nearly equal contributions from a 3% increase in N_X and a 1.5% decrease in N_{RJ} . This truncation uncertainty in H_0 is somewhat larger than Holzzapfel et al. (1997) found in their work on H_0 using cluster Abell 2163 — an increase in the derived value of H_0 of only 1% due to truncation. This is at least partially due to the very large radius ($\sim 18'$) to which the X-ray emission of Abell 2163 extends and over which the isothermal- β model is an excellent fit.

An even larger source of uncertainty in determining H_0 comes from the elliptical morphology of galaxy clusters. In the following we quantify this uncertainty numerically using our axisymmetric ellipsoidal models for the gas distribution of CL 0016+16. Employing equations (6)–(9) and the best-fit values in Tables 2 and 3, we arrive at the values in Table 5 for H_0 as a function of line-of-sight inclination angle. Even if the symmetry axis of the cluster is assumed to lie in the plane of the sky (inclination angle of $i = 90^\circ$), then whether the cluster is oblate or prolate introduces an uncertainty of approximately $\pm 8\%$ in H_0 compared to the circular model. In fact it is easy to see that for $i = 90^\circ$ the ratio of Hubble constants is $H_0(\text{oblate})/H_0(\text{prolate}) = e$, which comes directly from the different line-of-sight depths through the cluster under the two assumptions.

Results for different assumed values of the inclination angle of the symmetry axis of the cluster to the line-of-sight are shown graphically in Figure 6 and some numerical values are given in Table 5. We have chosen to plot H_0 versus the intrinsic major/minor axis ratio

of the cluster, rather than versus inclination angle, although the results are equivalent. Clearly the minimum intrinsic axis ratio is obtained when the cluster's symmetry axis lies in the plane of the sky, $i = 90^\circ$, which corresponds to the left side of Figure 6. As the symmetry axis of the ellipsoid is allowed to vary toward the line-of-sight ($i = 0^\circ$), then the intrinsic major/minor axis ratio grows increasingly larger, as does the uncertainty on H_0 . This appears in Figure 6 as the increasing difference between the prolate and oblate curves as the abscissa increases.

In the absence of other information about the structure of galaxy clusters, the error in H_0 from these geometric effects can be quite large. However, a reasonable method for bounding the H_0 error is to bound the range of observed, projected ellipticities of other clusters. Mohr et al. (1995) analyzed a sample of galaxy clusters, fitting elliptical isothermal- β models to their X-ray images, and found a mean value for the observed major/minor axis ratio of 1.25 ± 0.19 from the sample. Of course this is not a measurement of the intrinsic axial ratio of clusters, but it does indicate that highly elliptical clusters tend to be rare. Guided by these results we make the assumption that the intrinsic value of the major/minor axis ratio of an individual cluster is unlikely to be greater than 1.5 (this value is shown as the vertical dashed line in Figure 6) and find that the range of H_0 is then bounded to $40 - 51 \text{ km s}^{-1} \text{ Mpc}^{-1}$ if the cluster is oblate and $43 - 55 \text{ km s}^{-1} \text{ Mpc}^{-1}$ if the cluster is prolate. This total range is $\pm 17\%$ when expressed as a fractional error.

How might these results generalize to clusters with other values of observed ellipticity? Let us consider two extreme cases. The first case assumes that the cluster appears circularly symmetric. This might indicate that the cluster is indeed spherically symmetric, but it could also mean that the cluster is oblate or prolate with a symmetry axis lying directly along the line-of-sight. One needs to consider the latter situation in order to assess honestly the systematic error due to unknown geometry. Doing that we find the fractional error in H_0 to be $\pm 38\%$. In the second case we assume that the cluster has an observed major/minor axis ratio of 1.5, i.e., the cluster has the maximum intrinsic ellipticity and the symmetry axis lies in the plane of the sky. Now we find that the conservative error estimate, assuming oblate and prolate geometries, yields a fractional error in H_0 of $\pm 20\%$.

More definitive information about the intrinsic structures of clusters could significantly reduce these systematic errors. For example, if we could be certain that clusters were nearly always prolate, then the fractional errors associated with the two extreme cases presented above would be reduced to $\pm 20\%$ and 0% , respectively. Until more theoretical and observational studies give us such insights into the nature of galaxy clusters, the simplified arguments presented in the preceding paragraph should be kept in mind when considering the total error budget associated with X-ray/SZ-effect distance measurements.

4.4. Comparison with Other SZ-derived Values for the Hubble Constant

There are seven other galaxy clusters in addition to CL 0016+16 with published measurements of H_0 from the SZ effect based on various observational techniques. In the rest of this section we compare these results. When necessary and as indicated below, we have applied the appropriate relativistic corrections for the intensity of X-ray bremsstrahlung

emissivity and the inverse Compton scattering distortions to the CMBR using the techniques described above. We have made sure that the various H_0 values were determined in a consistent fashion with the same assumptions about the cluster structure and temperature distribution. With the exception of the Coma Cluster for which a nonisothermal temperature distribution was used, the values we present in Table 6 were determined assuming spherical symmetry; an isothermal- β model for the gas density distribution; isothermal, unclumped gas; and $\Omega_0 = 0.2$, $\lambda_0 = 0$. Uncertainties are nearly entirely observational and are given at the 1σ confidence level.

Myers et al. (1997) present results of SZ effect observations in four nearby clusters of galaxies from single dish measurements at 32 GHz with the OVRO 5.5-m telescope. In their analysis these authors include relativistic corrections for the SZ effect, but not for the X-ray bremsstrahlung emission, since their X-ray results come largely from the literature. For the mean cluster temperatures determined by *Ginga*, we find that the relativistically-corrected H_0 values are smaller than the Myers et al. values by 5.2% (A2256, A478), 5.4% (A2142), and 5.5% (Coma). The Myers et al. values also need to be increased slightly (adjustments range from 0.5% for Coma to 1.8% for A2142) for consistency with our different assumed cosmology.

The SZ detection of the Coma cluster was first reported by Herbig et al. (1995), whose analysis, as mentioned above, incorporated a nonisothermal temperature distribution as derived from various X-ray data sets by Hughes, Gorenstein, & Fabricant (1988). The general shape of the radial temperature variation of Coma is both strongly motivated and observationally secure (see Hughes 1997 for a summary of recent results and models), so Herbig et al.'s use of it is appropriate. Unfortunately, these authors do not quote an H_0 value for an isothermal temperature distribution, and it is not possible to estimate one from their article, so the sensitivity of the derived value of H_0 to the assumption of nonisothermality for the Coma Cluster cannot be assessed. We do not use Coma's H_0 value for the ensemble average in Table 6, but consider it later as discussed below.

Our published value of H_0 from the SZ effect of A2218 (65 ± 25 km s⁻¹ Mpc⁻¹, Birkinshaw & Hughes 1994) has been adjusted for relativistic corrections to the SZ effect (reduced by 4%) and X-ray bremsstrahlung emissivity (reduced by 5.2%) and for consistency with our different assumed cosmology (reduced by 1%). These same three corrections were applied to the result from Jones (1995) of $H_0 = 38_{-16}^{+18}$ km s⁻¹ Mpc⁻¹, which were based on interferometric SZ maps from the Ryle Telescope observing at 15 GHz and *ROSAT* PSPC X-ray images.

The result on A665 quoted in Table 6 comes from a detailed analysis of a deep *ROSAT* PSPC image (Hughes & Birkinshaw 1998) and uses the OVRO 40-m telescope SZ effect data from Birkinshaw et al. (1991). It has been corrected for relativistic effects and has been computed for the assumed cosmological parameters.

The SZ effect measurements of A2163 from an infrared bolometer array observing at 2.1 mm (SuZIE, the Sunyaev-Zel'dovich Infrared Experiment) and the *ROSAT* PSPC X-ray data were analyzed in a comprehensive article by Holzapfel et al. (1997). We have selected

their value of H_0 derived for an isothermal temperature distribution ($59.6_{-22.6}^{+40.7}$ km s $^{-1}$ Mpc $^{-1}$) and applied relativistic corrections for the X-ray bremsstrahlung emissivity (which reduced their value by 7.7%) and for our different assumed cosmology (which increased their value by 4%).

The ensemble average for $H_0 = 47.1 \pm 6.8$ km s $^{-1}$ Mpc $^{-1}$ was computed by minimizing χ^2 assuming the eight measurements (excluding Coma) are independent data points, and including the asymmetry of the error bars on the individual measurements. The assumption of independence is not strictly correct since the several observations share systematic errors and the two values from A2218 share the same measurement of the cluster temperature from *Ginga*. Nevertheless this procedure gives a mean value that is comparable to the weighted (45 km s $^{-1}$ Mpc $^{-1}$) or unweighted (49 km s $^{-1}$ Mpc $^{-1}$) average of the eight measurements. None of the individual results differs by more than 1.5σ from the ensemble average.

4.5. Systematic Errors and Biases

The excellent agreement among the various H_0 measurements quoted above notwithstanding, any serious attempt at determining cosmological parameters from the SZ effect demands a careful and intensive analysis of systematic effects that might be sources of error. We make an important distinction between systematic errors that may introduce a bias in an ensemble average value versus errors that may introduce a random uncertainty. The dominant sources of biases are calibration errors in the flux scale of X-ray measurements or the brightness temperature of the SZ effect measurements, large scale temperature gradients in cluster atmospheres, clumping of cluster gas, and a poorly selected sample of clusters. Random errors include primarily any motion of a cluster with respect to the Hubble flow and cluster morphology, such as the effects of ellipticity as studied in detail above. Clearly the effects of biases are particularly pernicious since they cannot be eliminated by increasing the size of the cluster sample. Rather, their effect on the derived value of H_0 must be carried along as an additional error term. In the following we draw upon work of others as well as our own to quantify these various systematic errors.

Birkinshaw & Hughes (1994) and Holzapfel et al. (1997) allowed for large scale radial temperature gradients when analyzing the SZ effect and X-ray data for A2218 and A2163, respectively. Both groups found that, for temperature profiles that fell with radius (as is the case for the temperature profile of the Coma cluster), the value of H_0 derived under an isothermal assumption would underestimate the true H_0 value by 20%–30%. Inagaki, Suginozono, & Sato (1995) came to a similar conclusion based on studies of simulated clusters with temperature distributions that fell with radius. Our own comparison of H_0 measurements in Table 6 also bears this out to some extent. Specifically the best-fit value of H_0 from the Coma Cluster, for which a nonisothermal temperature distribution was used, is about 36% greater than the ensemble average of the other clusters, for which the gas was assumed to be isothermal.

If cluster gas is clumped, then X-ray emissivity will be increased relative to SZ by a factor greater than unity (BHA). In this case the value of H_0 derived assuming an

unclumped gas distribution will be an upper limit to the true H_0 value. Holzapfel et al. (1997) used X-ray spectral fits to constrain the amount of isobaric clumping in A2163 and found that a reduction in H_0 of only $\sim 10\%$ from the unclumped case was allowed.

The peculiar motion of clusters relative to the Hubble flow introduces an additional distortion to the CMBR spectrum usually referred to as the “kinematic” SZ effect. For a cluster with a peculiar velocity of 1000 km s^{-1} and temperature of 10 keV the strength of the kinematic SZ effect would be $\sim 9\%$ of the thermal effect in the Rayleigh-Jeans portion of the CMBR spectrum (BHA). Recently Watkins (1997) presented observational evidence that argues for a low 1-D RMS peculiar velocity of clusters, $\sigma_v \sim 300 \text{ km s}^{-1}$. Assuming this value and recalling that the SZ effect intensity enters as a square in the equation determining H_0 , we determine that the kinematic SZ effect could introduce up to a $\sim \pm 8\%$ correction in the measurement of H_0 from any individual cluster (for $kT_{e0} = 7 \text{ keV}$). It is important to note that this effect produces a spectral signature that is different from the thermal effect and so, in principle, is amenable to observation. In practice, current results are not sensitive enough to set significant constraints; the SuZIE observations of A2163 constrain its 1-D peculiar velocity to be less than 1500 km s^{-1} . Peculiar velocities are unlikely to be correlated for clusters that are widely distributed in redshift and position, so this effect would result in an additional random uncertainty in H_0 for any single cluster.

The effect of cluster ellipticity that we have studied in some detail in this article tends to introduce a random uncertainty of about $\pm 20\%$ in H_0 for an average cluster. However, to ensure that these effects of unknown geometry and arbitrary inclination are uncorrelated from cluster to cluster, it is essential that the cluster sample for determining H_0 be selected properly. For example, as pointed out by BHA, it is important that clusters *not* be selected based on the strength of their SZ effect signal or central X-ray surface brightness, since this would result naturally in a bias toward prolate clusters with their long axes aligned to the line-of-sight. As figure 6 clearly shows, this bias would cause the derived value of H_0 to be an underestimate of the true value. The four low redshift objects in Table 6 are part of an X-ray flux-limited sample of nearby clusters that are being studied in the SZ effect (Myers et al. 1997). The four other clusters are part of a moderate redshift sample selected on the strength of their integrated X-ray flux from surveys by the *Einstein Observatory* or *ROSAT* that we and our collaborators have been observing in the X-rays and SZ effect. Although the entire sample in each case should be relatively unbiased, it is not clear that the same may be said about the subsamples presented here. A definitive answer awaits the final analysis of the entire sample.

We take account of the systematic errors mentioned above by quoting a range in H_0 that includes a bias of $+30\%$ from large scale temperature gradients and one of -10% from clumping in the cluster gas. Additional random systematic errors on the ensemble average are $\pm 3\%$ from peculiar motion and $\pm 7\%$ from unknown geometry/inclination, which the reader will note have been reduced from the values given above by $1/\sqrt{N}$ where $N = 8$ is the number of clusters in the sample. These random errors are then root-sum-squared

with the 14% error on the ensemble average quoted in Table 6. This yields a best estimate of the Hubble constant from the Sunyaev-Zel'dovich effect of

$$H_0 = 42 - 61 \text{ km s}^{-1} \text{ Mpc}^{-1} \pm 16\%. \quad (13)$$

5. CONCLUSIONS

In this article we have arrived at the following conclusions.

- (1) The structure of the intracluster medium of CL 0016+16 is well described by a gas distribution that produces in projection an elliptical isothermal- β model with $\beta \approx 0.74$, $\theta_C \approx 0.75$ arcmin (along the major axis), and observed major/minor axis ratio ≈ 1.18 with the major axis lying at position angle $\approx 51^\circ$ measured east of north.
- (2) If the cluster is assumed to be spherically-symmetric and isothermal, then we derive a value for the Hubble constant of $H_0 = 47_{-15}^{+23} \text{ km s}^{-1} \text{ Mpc}^{-1}$. The error includes random uncertainties from fits to the model parameters and systematic uncertainties in background subtraction (for *ASCA* spectroscopy), the overall *ROSAT* X-ray flux calibration, and the brightness temperature scale of the OVRO 40-m telescope. An additional, one-sided error of $+21 \text{ km s}^{-1} \text{ Mpc}^{-1}$ comes from the zero level uncertainty.
- (3) We have quantified the error in H_0 from unknown geometry and line-of-sight inclination angle effects, under the assumption that CL 0016+16 is an axisymmetric ellipsoidal system. The H_0 error can be bounded if we assume that the intrinsic major/minor axis ratio of the cluster is less than 1.5. In this case we find (not including observational errors)

$$\begin{aligned} \text{Oblate : } H_0 &= 40 - 51 \text{ km s}^{-1} \text{ Mpc}^{-1} \\ \text{Prolate : } H_0 &= 43 - 55 \text{ km s}^{-1} \text{ Mpc}^{-1}. \end{aligned}$$

These ranges represent an irreducible uncertainty in the value of H_0 as determined from this single cluster, and indicate the sizes of the errors that would be caused by reasonable triaxial models for the cluster. In the more general case of an arbitrary observed ellipticity we find that the fractional error associated with H_0 is probably not much smaller than $\pm 15\%$ and in the worst case may be as large as $\pm 38\%$.

- (4) At the redshift of CL 0016+16, $z = 0.5455$, the effects of the cosmological parameters on the derived value of H_0 can be of order 10%–20%. The results given above are for a Friedmann Universe with $q_0 = 0.1$. Turning the problem around and assuming that the results summarized in item (3) above can be applied to other clusters, in order to place significant constraints on the cosmological parameters using the SZ effect it will be necessary to utilize a carefully selected sample of ~ 20 or more clusters at redshifts beyond ~ 0.2 .
- (5) When the result for CL 0016+16 given here is compared with other determinations of H_0 from the SZ effect (see Table 6), a consistent ensemble value of $47 \pm 7 \text{ km s}^{-1} \text{ Mpc}^{-1}$ is obtained under the assumption of a spherical, unclumped, isothermal cluster atmosphere. This mean value depends only slightly on the assumed cosmology varying

by ${}_{-1.4}^{+2.6}$ km s⁻¹ Mpc⁻¹ for the extreme curves shown in Figure 5. Inclusion of likely systematic errors increases the allowed range of H_0 to 42 – 61 km s⁻¹ Mpc⁻¹ with a random error of $\pm 16\%$. It is reassuring that this result is consistent with other independent measures of H_0 such as those from using Type Ia supernovae (SNe) as standard candles: 62–67 km s⁻¹ Mpc⁻¹ (Hamuy et al. 1995) and 67 ± 7 km s⁻¹ Mpc⁻¹ (Riess, Press, & Kirshner 1996); the expanding photosphere method on Type II SNe 73 ± 7 km s⁻¹ Mpc⁻¹ (Schmidt et al. 1994); or from measurements of time delays in gravitational lenses: 64 ± 13 km s⁻¹ Mpc⁻¹ (Kundić et al. 1997) and 41 – 84 km s⁻¹ Mpc⁻¹ (Schechter et al. 1997).

- (6) The dominant source of error in the determination of H_0 from the SZ effect is the possible existence of large scale radial temperature gradients in cluster atmospheres. It is interesting to note that the presence of negative radial gradients, similar to the kind observed in the Coma cluster, is roughly what is needed to bring the low values of H_0 determined assuming isothermal atmospheres into agreement with the results from supernovae mentioned above. The temperature distribution of clusters can be studied observationally by comparing interferometric maps of the SZ effect (which sample $n_e T_e$) with X-ray images (which effectively sample n_e^2) or through direct spatially resolved X-ray spectral measurements with the upcoming satellites *AXAF* and *XMM*. Over the next few years we expect to make substantial progress in resolving this key issue.

Acknowledgements

This research has made use of data obtained through the High Energy Astrophysics Science Archive Research Center Online Service, provided by the NASA/Goddard Space Flight Center. JPH was partially supported by NASA *ROSAT* Grant NAG5-2156 and NASA Long Term Space Astrophysics Program Grant NAG5-3432. MB was partially supported by NASA grants NAGW-3825 and NAG5-2415, NASA contract NAS8-39073, and a PPARC grant.

REFERENCES

- Birkinshaw, M. 1979, MNRAS, 187, 847
- Birkinshaw, M. 1998, Physics Reports, in press.
- Birkinshaw, M., Gull, S.F., Hardebeck, H.E. & Moffet, A.T., 1997, ApJ, submitted.
- Birkinshaw, M., Hughes, J. P., & Arnaud, K. A. 1991, ApJ, 379, 466 (BHA)
- Birkinshaw, M., & Hughes, J. P. 1994, ApJ, 420, 33
- Briel, U. G., Henry, J. P., and Böhringer, H. 1992, *a*, 259, 131
- Carlberg, R. G., Yee, H. K. C., Ellingson, E., Abraham, R., Gravel, P., Morris, S., & Pritchett, C. J. 1996, ApJ, 462, 32
- Carlstrom, J. E., Joy, M., & Grego, L. 1996, ApJ, 456, L75
- Carroll, S. M., Press, W. H., & Turner, E. L. 1992, ARA&A, 30, 499
- Cavaliere, A., Danese, L., & DeZotti, G. 1979, *a*, 75, 322
- Dressler, A., & Gunn, J. E. 1992, ApJS, 78, 1
- Fabricant, D., Rybicki, G., & Gorenstein, P. 1984, ApJ, 286, 186
- Fixsen, D. J., Cheng, E. S., Gales, J. M., Mather, J. C., Shafer, R. A. & Wright, E. L. 1996, ApJ, 473, 576
- Gould, R. J. 1980, ApJ, 238, 1026; erratum 243, 677 (1981)
- Gunn, J. E. 1978, in *Observational Cosmology*, eds. A. Maeder, L. Martinet, & G. Tamman (Geneva: Geneva Observatory)
- Hamuy, M., Phillips, M. M., Maza, J., Suntzeff, N. B., Schommer, R., & Aviles, A. 1995, AJ, 109, 1
- Hasinger, G., Turner, T. J., George, I. M., & Boese, G. 1992, Legacy, 2, 77
- Herbig, T., Lawrence, C. R., Readhead, A. C. S., & Gulkis, S. 1995, ApJ, 449, L5
- Holzappel, W. L., Arnaud, M., Ade, P. A. R., Church, S. E., Fischer, M. L., Mauskopf, P. D., Rephaeli, Y., Wilbanks, T. M., & Lange, A. E. 1997, ApJ, 480, 449.
- Hughes, J. P. 1997, in the Proceedings of the conference *A New Vision of an Old Cluster: Untangling Coma Berenices* (held June 17-20, Marseille, France), in press (astro-ph/9709272).
- Hughes, J. P., & Birkinshaw, M. 1998, ApJ, in preparation
- Hughes, J. P., Birkinshaw, M., & Huchra, J. P. 1995, ApJ, 448, L93
- Hughes, J. P., Butcher, J. A., Stewart, G. C., & Tanaka, Y. 1993, ApJ, 404, 611
- Hughes, J. P., Gorenstein, P., and Fabricant, D. 1988, ApJ, 329, 82
- Inagaki, Y., Sugihara, T., & Suto, Y. 1995, PASJ, 47, 411
- Jones, M. 1995, Astrophys. Lett. & Comm., 32, 1-6, 347
- Karzas, W., and Latter, R. 1961, ApJS, 6, 167

- Kendall, M., & Stuart, A. 1979, *The Advanced Theory of Statistics, Volume 2* (New York: Macmillan), 246ff
- Kobayashi, S., Sasaki, S., & Suto, Y. 1996, *PASJ*, 48, 107
- Kundić, T., et al. 1997, *ApJ*, 482, 75
- Madore, B. F., et al. 1996, *BAAS*, 28, 1420
- Margon, B., Downes, R. A., & Spinrad, H. 1983, *Nature*, 301, 221
- Moffet, A. T., & Birkinshaw, M. 1989, *AJ*, 98, 1148
- Mohr, J. J., Evrard, A. E., Fabricant, D. G., & Geller, M. J. 1995, *ApJ*, 447, 8
- Myers, S. T., Baker, J. E., Readhead, A. C. S., & Herbig, T. 1997, *ApJ*, 485, 1
- Ohashi, T., et al. 1996, *PASJ*, 48, 157
- Perlmutter, S., et al. 1997, *ApJ*, 483, 565
- Pfeffermann, E., et al. 1986, *Proc. SPIE Int. Opt. Eng.*, 733, 519
- Press, W. H., Flannery, B. P., Teukolsky, S. A., & Vetterling, W. T. 1985, *Numerical Recipes, Ed. 1* (Cambridge: Cambridge University Press), 289
- Rephaeli, Y., & Yankovitch, D. 1997, *ApJ*, 481, L55
- Riess, A. G., Press, W. H., & Kirshner, R. P. 1996, *ApJ*, 473, 88.
- Rybicki, G. B., & Lightman, A. P. 1979, *Radiative Processes in Astrophysics* (New York: Wiley), p. 165
- Schechter, P. L., et al. 1997, *ApJ*, 475, L85
- Schmidt, B. P., et al. 1994, *ApJ*, 432, 42
- Silk, J., & White, S. D. M. 1978, *ApJ*, 226, L103
- Stark, A. A., Heiles, C., Bally, J., & Linke, R. 1984, privately distributed magnetic tape
- Tanaka, Y., Inoue, H., & Holt, S. S. 1994, *PASJ*, 46, L37
- Trümper, J. 1983, *Adv. Space Res.*, 2(4), 241
- van den Bergh, S. 1995, *ApJ*, 453, L55
- Weinberg, S. 1972, *Gravitation and Cosmology* (Wiley: New York), 485
- Yamashita, K. 1994, in *New Horizon of X-Ray Astronomy—First Results from ASCA*, ed. F. Makino & T. Ohashi (Tokyo: Universal Academy), 279

TABLE 1
CIRCULAR ISOTHERMAL- β MODEL FIT

Parameter	Fitted Value	Error ^a
PSPC X-ray Data		
R.A. (J2000)	0 ^h 18 ^m 33.18 ^s	$\pm 0.05^s$
Decl. (J2000)	16°26'17".9	$\pm 0.8''$
β	0.728	+0.025 -0.022
θ_C (')	0.679	+0.045 -0.039
$b_X(0)$ (counts s ⁻¹ arcmin ⁻²)	4.71×10^{-2}	$\pm 0.24 \times 10^{-2}$
OVRO SZ Effect Data		
$\Delta T_{RJ}(0)$ (μ K)	-1205	± 190

^a Single parameter 1- σ errors

TABLE 2
 ELLIPTICAL ISOTHERMAL- β MODEL FIT

Parameter	Fitted Value	Error ^a
PSPC X-ray Data		
R.A. (J2000)	0 ^h 18 ^m 33.18 ^s	$\pm 0.05^s$
Decl. (J2000)	16°26'17".8	$\pm 0.8''$
β	0.737	+0.027 -0.022
θ_C (') (along major axis)	0.746	± 0.044
e ^b	1.176	+0.033 -0.030
Position angle (°)	50.8	± 4.9
$b_X(0)$ (counts s ⁻¹ arcmin ⁻²)	4.72×10^{-2}	$\pm 0.24 \times 10^{-2}$
OVRO SZ Effect Data		
$\Delta T_{RJ}(0)$ (μ K)	-1207	± 190

^a Single parameter 1- σ errors

^b Defined as observed major axis divided by minor axis

TABLE 3
JOINT PSPC/GIS SPECTRAL MODEL FIT

Parameter	Fitted Value	Error ^a
Cluster: CL0016+16 (Thermal Model)		
kT (keV) ^b	7.55	$+0.72$ ^c -0.58
$[\text{Fe}]/[\text{H}]$ ^d	0.07	$+0.11$ -0.07
N_{H} (atoms cm^{-2})	5.59×10^{20}	$+0.41$ -0.36 $\times 10^{20}$
Emission Measure ^e (cm^{-5})	3.65×10^{11}	$\pm 0.09 \times 10^{11}$
AGN: QSO 0015+162 (Power-law Model)		
α_p	2.54	± 0.18
$F_{1\text{keV}}$ (photons $\text{keV}^{-1} \text{cm}^2 \text{s}^{-1}$)	5.14×10^{-5}	$+0.43$ -0.39 $\times 10^{-5}$

^a Single parameter $1\text{-}\sigma$ errors

^b Source frame for $z = 0.5455$

^c RSS of $+0.63$ (statistical error) and $+0.35$ ($\pm 6\%$ background subtraction error)

^d Relative to solar $[\text{Fe}]/[\text{H}] = 4 \times 10^{-5}$

^e Flux (0.2–2.0 keV) = 1×10^{-12} ergs $\text{cm}^{-2} \text{s}^{-1}$

Flux (2–10 keV) = 1.5×10^{-12} ergs $\text{cm}^{-2} \text{s}^{-1}$

TABLE 4
 UNCERTAINTY IN H_0 FROM OBSERVATIONAL ERRORS

	kT	[Fe]/[H]	N_{H}	β	θ_C	$b_X(0)$	$\Delta T_{RJ}(0)$
Observational Error ^a (%)	+9.5 -7.7	+157 -100	+7.3 -6.4	+3.4 -3.0	+6.6 -5.7	± 5.1	± 15.7
δH_0 ^a km s ⁻¹ Mpc ⁻¹	+9.5 -7.0	-1.0 +0.6	± 0.5	————	± 2.0 ^b ———	————	-11.8 +18.8

^a 1- σ errors

^b Over three-dimensional error surface for β , θ_C , and $b_X(0)$

TABLE 5
 UNCERTAINTY IN H_0 FROM UNKNOWN GEOMETRY

Model	H_0 (km s ⁻¹ Mpc ⁻¹)	
	Oblate	Prolate
Circular	47.2	
Inclination angle 90°	50.7	43.1
Inclination angle 70°	49.4	43.9
Inclination angle 50°	43.3	47.2
Intrinsic major/minor axis ratio 1.5	39.7	55.0

TABLE 6
 SUMMARY OF X-RAY/SZ EFFECT H_0 MEASUREMENTS FOR
 SPHERICALLY SYMMETRIC, ISOTHERMAL CLUSTER MODELS

Cluster	z	H_0^a ($\text{km s}^{-1} \text{Mpc}^{-1}$)	Reference
Coma	0.0232	64^{+25}_{-21} ^b	Myers et al. 1997
Abell 2256	0.0581	69^{+21}_{-18}	Myers et al. 1997
Abell 478	0.0881	31^{+17}_{-13}	Myers et al. 1997
Abell 2142	0.0899	46^{+41}_{-28}	Myers et al. 1997
Abell 2218	0.171	59 ± 23	Birkinshaw & Hughes 1994
Abell 2218	0.171	34^{+16}_{-14}	Jones 1995
Abell 665	0.182	46 ± 16	Hughes & Birkinshaw 1998
Abell 2163	0.201	58^{+39}_{-22}	Holzappel et al. 1997
CL 0016+16	0.5455	47^{+23}_{-15}	This work
Ensemble average ^c	...	47.1 ± 6.8	...

^a Assuming $\Omega_0 = 0.2, \lambda_0 = 0$; uncertainties quoted at 1σ

^b Derived assuming a nonisothermal cluster temperature distribution

^c Not including Coma

FIGURE CAPTIONS

Fig. 1— A portion of the 0.4-2.4 keV *ROSAT* PSPC X-ray image centered on the distant cluster CL 0016+16 ($z = 0.5455$). Coordinates are quoted in epoch J2000. The grayscale shows the number of raw counts detected in each $7''.5$ square pixel ranging from a minimum of 1 (in source-free regions of the map) to a peak of 38 (near the center of the cluster). The contours show the background subtracted, exposure corrected data after adaptive smoothing. Contour levels start at 2.4×10^{-4} counts s^{-1} arcmin $^{-2}$ (approximately the average background level near the center of the detector) and increase by multiplicative factors of 1.75. The bright X-ray source immediately to the north of the cluster is an AGN, QSO 0015+162, at a redshift $z = 0.554$ (Margon et al. 1983). The recently discovered poor cluster, RXJ0018.3+1618, that is a companion to CL 0016+16 (Hughes et al. 1995), is partially visible to the southwest.

Fig. 2— *ROSAT* PSPC and *ASCA* GIS spectral data and best-fit models. The cluster was fit with a thermal emission model with variable abundances and line-of-sight absorption. The AGN, QSO 0015+162, was assumed to have a power-law spectral form with the same absorption as the cluster. CL 0016+16 and the AGN were resolved in the *ROSAT* data, so separate PSPC spectra were extracted and fit. However, these sources were not resolved by *ASCA* and only a single GIS spectrum was extracted (from a $5'$ radius region centered on CL 0016+16). The sum of the cluster model and AGN model was fit to the GIS data.

Fig. 3— The Sunyaev-Zel'dovich effect data for several points on a NS line through CL 0016+16. The declination offsets for each point are measured relative to a nominal cluster center at $00^{\text{h}}18^{\text{m}}34^{\text{s}}$, $16^{\circ}26'20''$. The error bars contain contributions from the uncertainties in point-by-point systematic errors, such as the radio source corrections that have been applied (and which are large for the southernmost two points in the scan). The horizontal lines indicate the $\pm 1\sigma$ error range on the estimated zero level offset. The best-fit spherical model for the cluster gas consistent with the X-ray image is shown by the dashed lines, which correspond to the best-fit normalization N_{RJ} and its $\pm 1\sigma$ errors.

Fig. 4— Comparison of the radial X-ray profiles of the best-fitting elliptical isothermal- β model with the *ROSAT* PSPC data integrated within azimuthal quadrants as labelled. The background level is indicated by the horizontal dashed line, the cluster emission is the dotted curve, and the solid histogram is the sum of these. The cluster emission is above background within a radius of $\sim 3'$. The smaller panels beneath each radial surface brightness plot show the residuals (in units of σ : data minus model divided by the statistical error) from the fits of the elliptical isothermal- β model.

Fig. 5— The effect of the cosmological parameters Ω_0 and λ_0 on the derived value of H_0 . The function f parameterizes the ratio of H_0 determined assuming a Friedmann model with $\Omega_0 = q_0 = 0$ to that with arbitrary Ω_0 and cosmological constant λ_0 .

Fig. 6— Variation of the derived value of the Hubble constant, H_0 , with the intrinsic major/minor axis ratio of CL 0016+16 for oblate and prolate geometries. This plot assumes that the three dimensional structure of the cluster is given by an ellipsoid of revolution with symmetry axis lying at different angles of inclination to the line of sight. For intrinsic major/minor axis ratio values on the left hand side of the figure, the symmetry axis lies near the plane of the sky ($i = 90^\circ$). For an intrinsic axis ratio of 1.5 (indicated by the vertical dotted line) the inclination angles are $i = 45^\circ$ (oblate) and $i = 34^\circ$ (prolate).

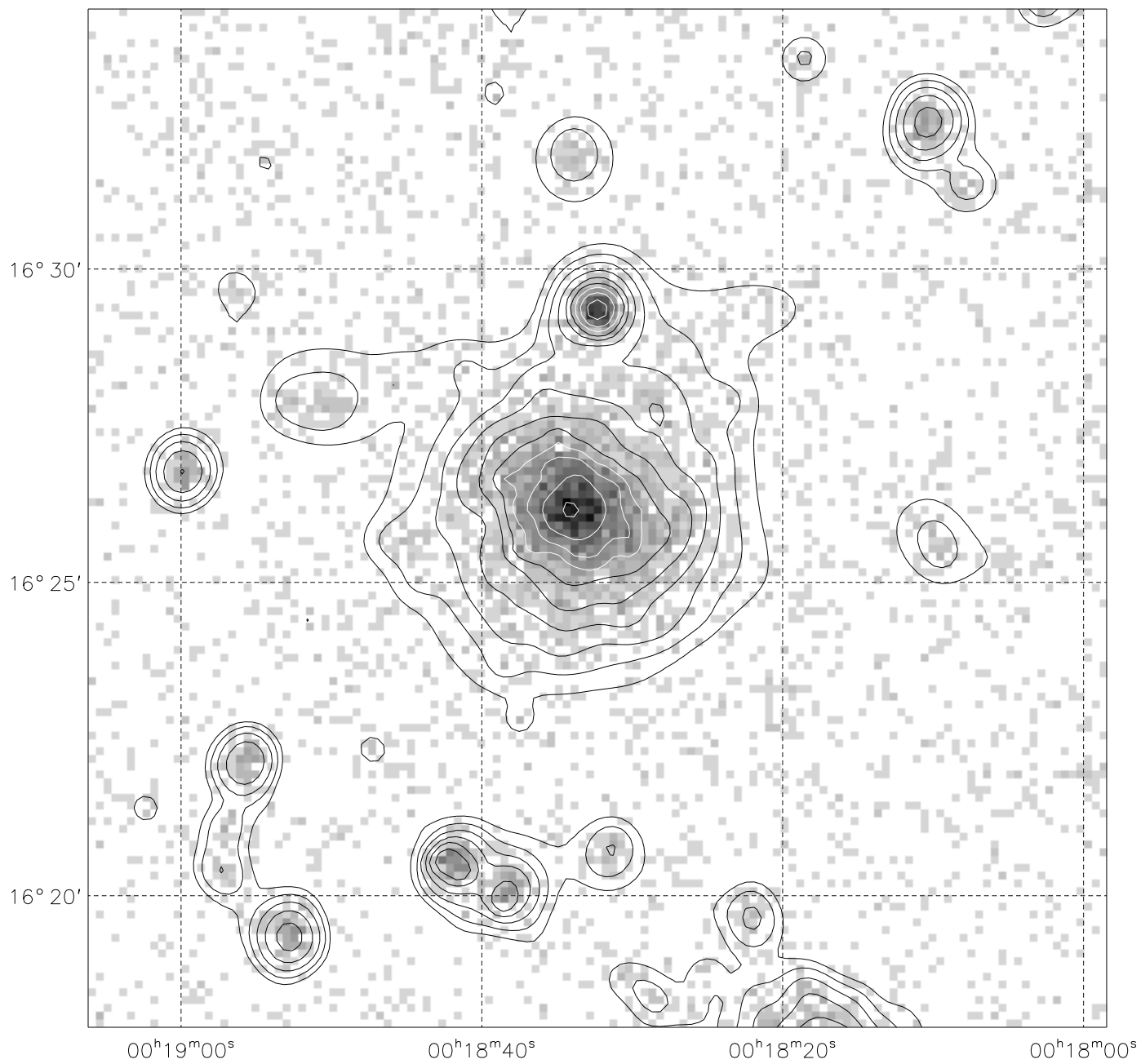


Figure 1

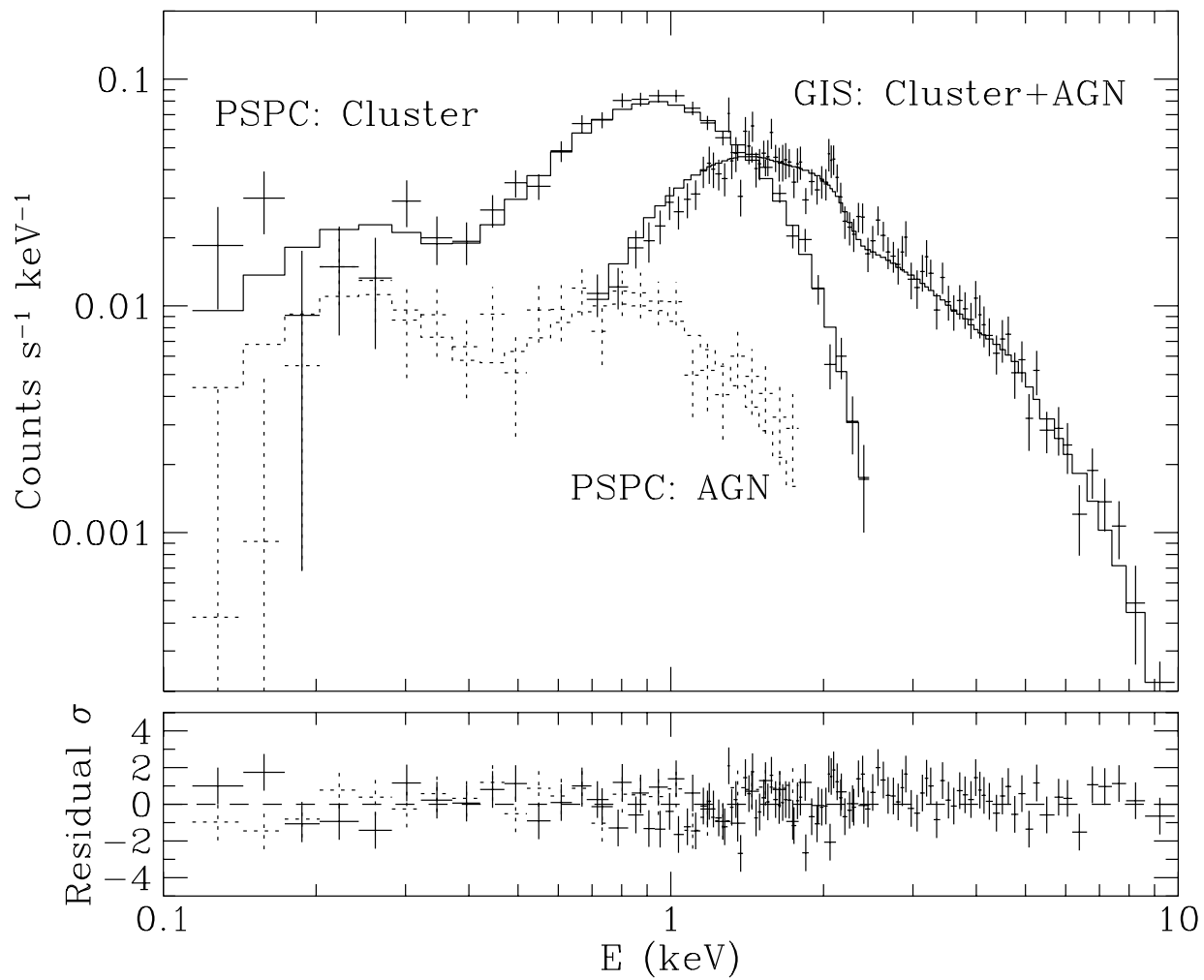


Figure 2

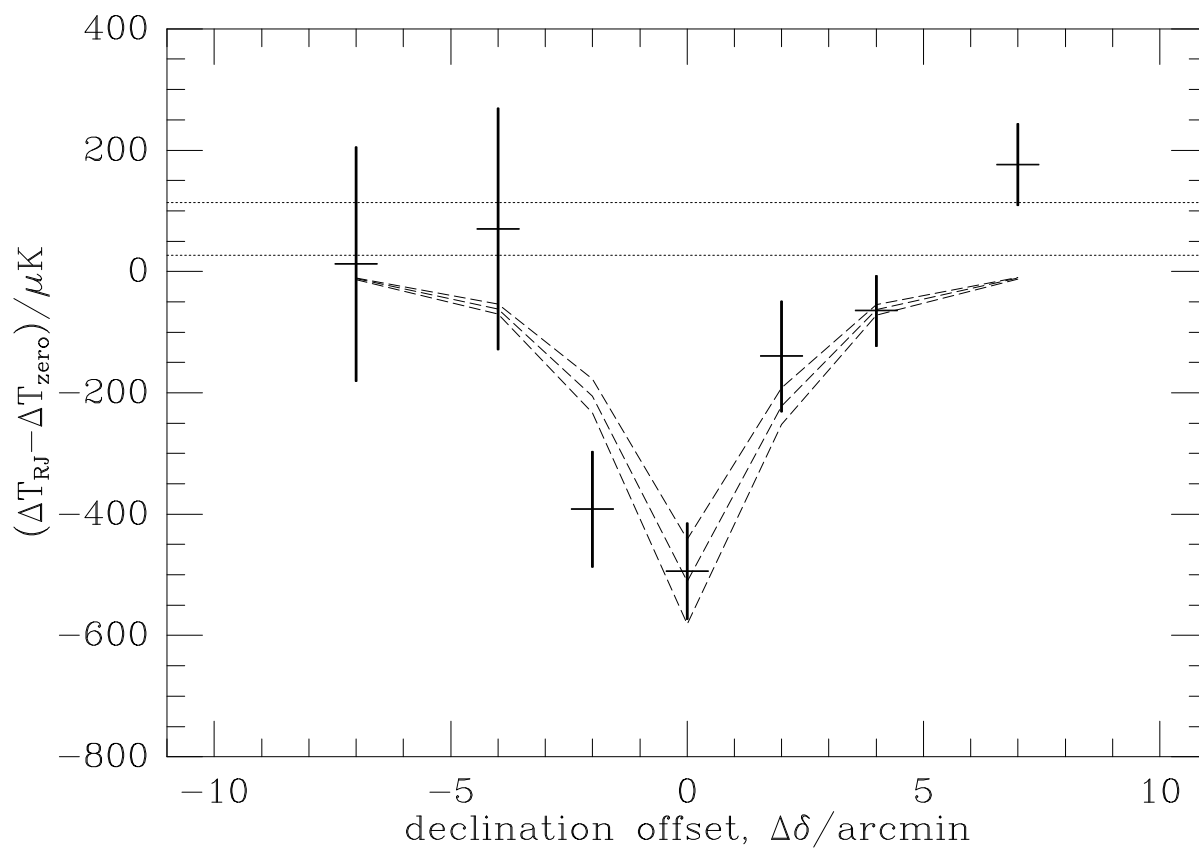


Figure 3

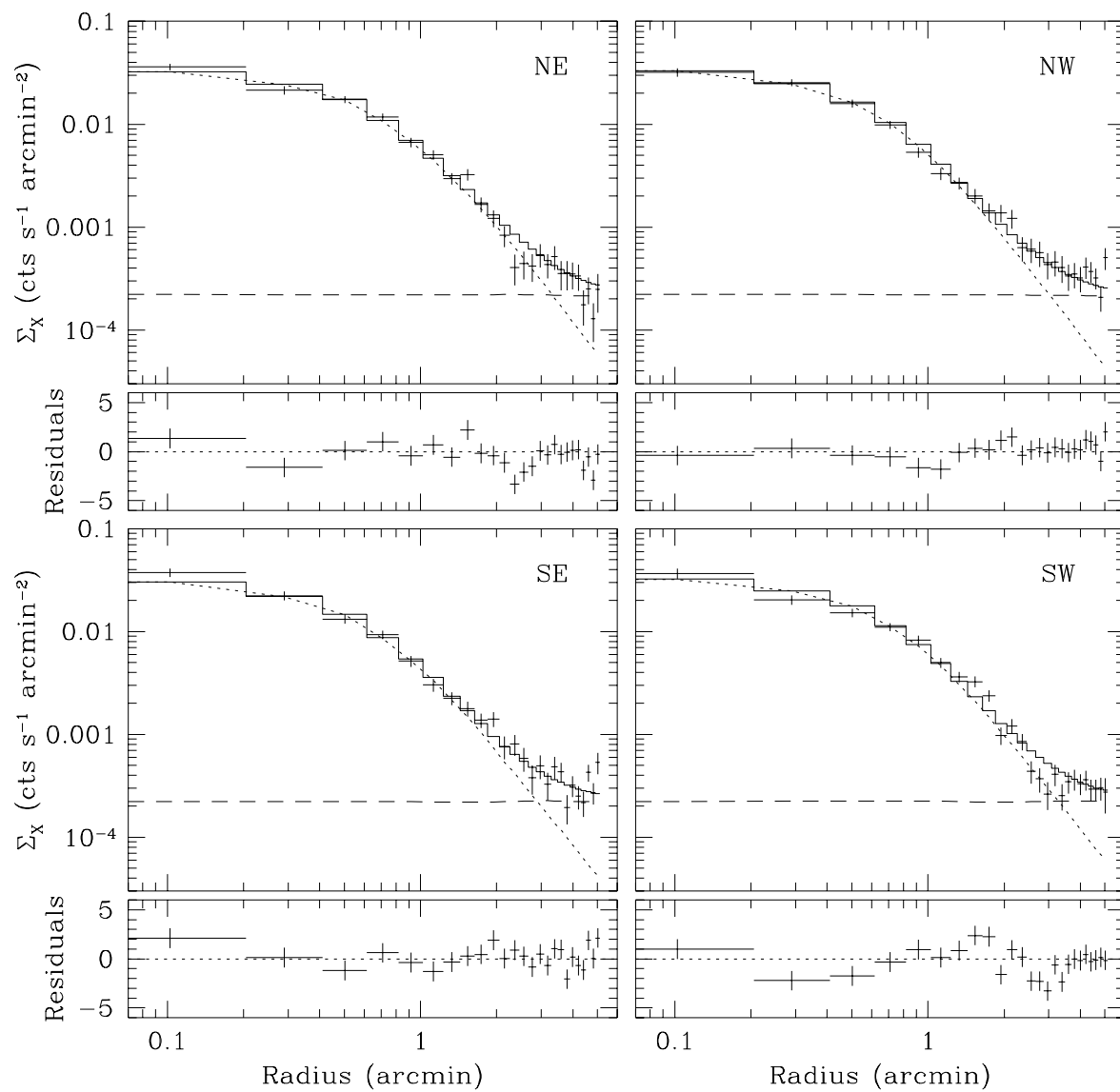


Figure 4

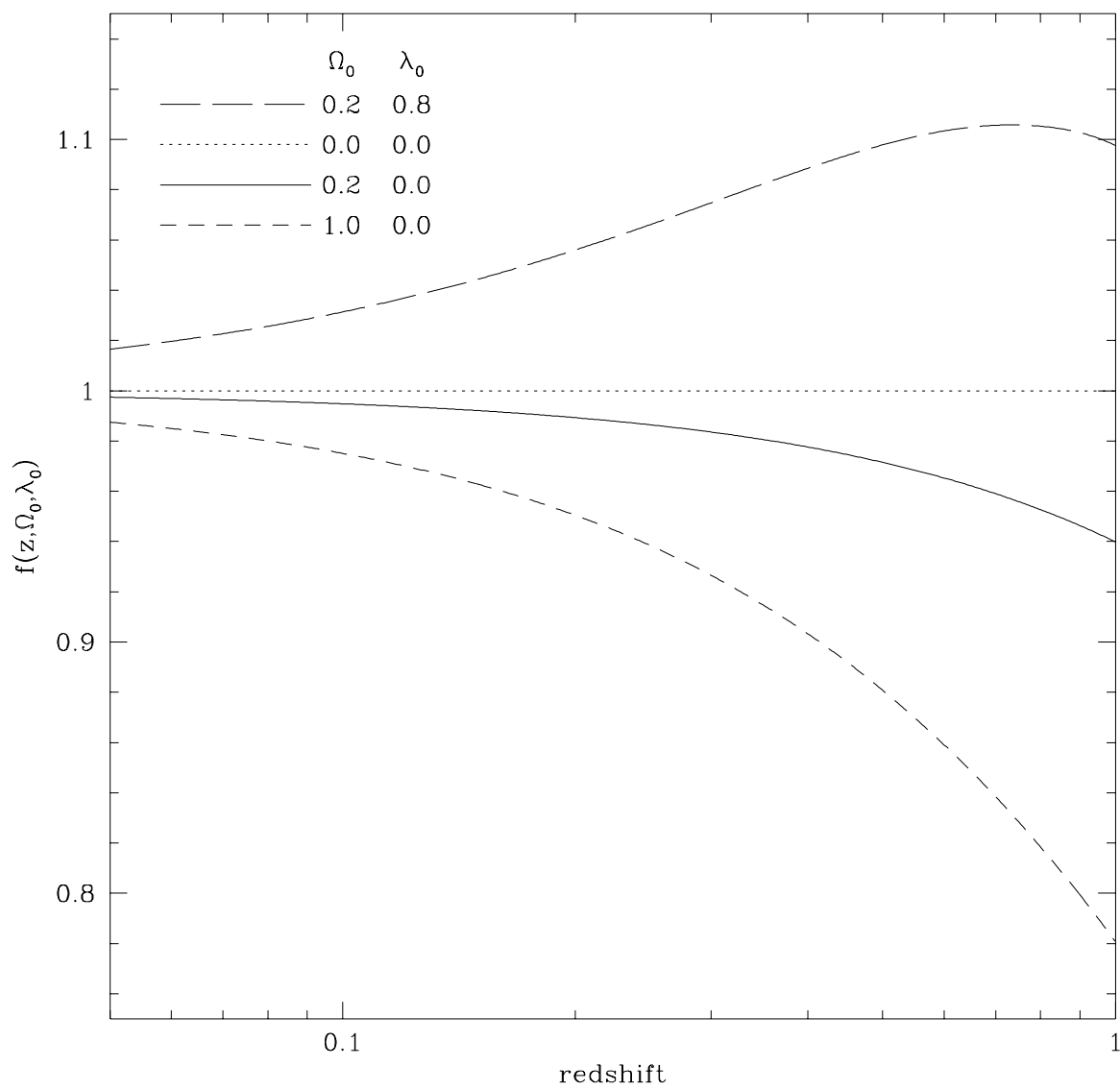


Figure 5

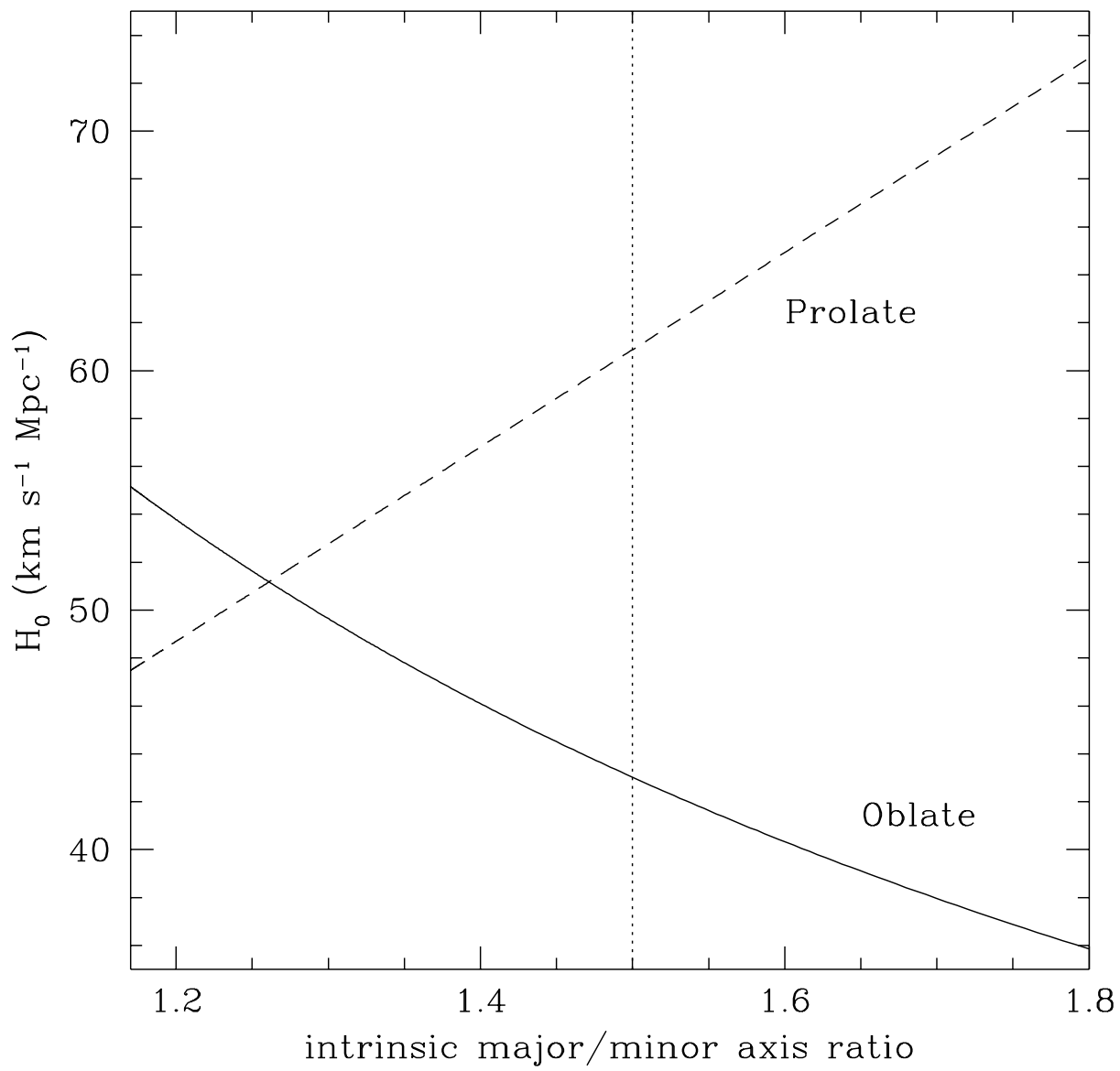


Figure 6